Thermodynamic Stability of Hydrogen-Bonded Nanostructures: A Calorimetric Study

Mattijs G. J. ten Cate, Jurriaan Huskens, Mercedes Crego-Calama,* and David N. Reinhoudt*[a]

Abstract: The self-assembly of hydrogen-bonded aggregates (rosettes) in solvent mixtures of different polarity has been studied by calorimetry. The C_{50} parameter, the concentration when 50% of the components are incorporated in the assembly, is used to compare assemblies with different stoichiometry. C_{50} for the single rosette $\mathbf{1}_3$·(BuCYA)$_3$ (**1** = *N*,*N*-di(4-*tert*-butylphenyl)melamine; BuCYA = *n*-butylcyanuric acid) in 1,2-dichloroethane is 25 μM, whereas for double rosettes $\mathbf{2a}_3$·(BuCYA)$_6$ and $\mathbf{2b}_3$·(BuCYA) (**2** = calix[4]arene–dimelamine) it is 0.7 and 7.1 μM, respectively. $\Delta G°$, $\Delta H°$, and $T\Delta S°$ values indicate that the thermodynamics of double rosettes reflect the independent assembly of two individual single rosette structures or two rosettes reinforced by additional stabilizing interactions. In more polar solvents the stability of double rosettes decreases. From the correlation of $\Delta G°$ with solvent polarity it is predicted that it should be possible to assemble double rosettes in methanol or water. The assembly of $\mathbf{2b}_3$·(BuCYA)$_6$ in 100% MeOH was proven by ^{1}H NMR and CD spectroscopy.

Keywords: calorimetry · hydrogen bonds · polar solvents · self-assembly · thermodynamics

Introduction

Because of the weak nature of the hydrogen bond (2–10 kcal mol^{-1}),[1] self-assembly in polar solvents has received little attention. Most self-assembly studies in polar solvents are carried out by using metal coordination[2–14] or a combination of hydrogen bonding with other weak noncovalent interactions, such as cation–π and π–π stacking, which has led to molecular capsules stable in polar organic solvents.[15–17] Furthermore, multiple ionic interactions have been used to obtain stable supramolecular complexes in polar solvents.[18–23] Polar solvents such as methanol and water can act as hydrogen-bond donors and acceptors, thereby competing for hydrogen bonding during assembly formation. This results in a decrease in stability of the hydrogen-bonded assemblies.

Whitesides and co-workers predicted qualitatively the stabilities of multiparticle hydrogen-bonded aggregates based on the numbers of hydrogen bonds and of particles.[24] Three indices, I_{Tm}, I_G and $I_G/(n-1)$, were introduced to estimate relative stabilities of hydrogen-bonded aggregates based on a rosette motif. I_{Tm} is directly related to the number of hydrogen bonds and the number (n) of particles, and has been shown to be the most valuable. I_G corresponds to a free energy of assembly, and assumes an average net enthalpy of formation of each hydrogen bond in the solvent of interest[25] and an average translational and rotational energy. $I_G/(n-1)$ corresponds to a free energy of association per particle. These indices are useful for estimating qualitatively the relative stability of different aggregates with similar hydrogen-bonding patterns, but they identify neither differences in hydrogen-bond strength within comparable assemblies, nor differences in stability due to steric strain or electronic influences induced by substituents present in the assembly.

Here we describe quantitatively the thermodynamics of the self-assembly of hydrogen-bonded single and double rosettes in solvent mixtures of different polarities. We have analyzed the energetic parameters for the formation of single rosette assemblies as reported by Whitesides and co-workers in apolar solvents,[26] and we have compared the data with those for the larger double rosette.

The single rosette $\mathbf{1}_3$·(BuCYA)$_3$ (Scheme 1a), assembled from three *N*,*N*-di(4-*tert*-butylphenyl)melamine (**1**) molecules and three *n*-butylcyanuric acid (BuCYA) molecules, has six DAD–ADA (D = donor, A = acceptor) interactions with a total of 18 hydrogen bonds formed.

The double rosette motif involves calix[4]arenes diametrically substituted at the upper rim with two functionalized

[a] M. G. J. ten Cate, J. Huskens, M. Crego-Calama, D. N. Reinhoudt
Laboratory of Supramolecular Chemistry and Technology
MESA$^+$ Institute for Nanotechnology
University of Twente, PO Box 217
7500 AE Enschede (The Netherlands)
Fax: (+31)53-4894645
E-mail: m.cregocalama@utwente.nl

  DOI: 10.1002/chem.200400085

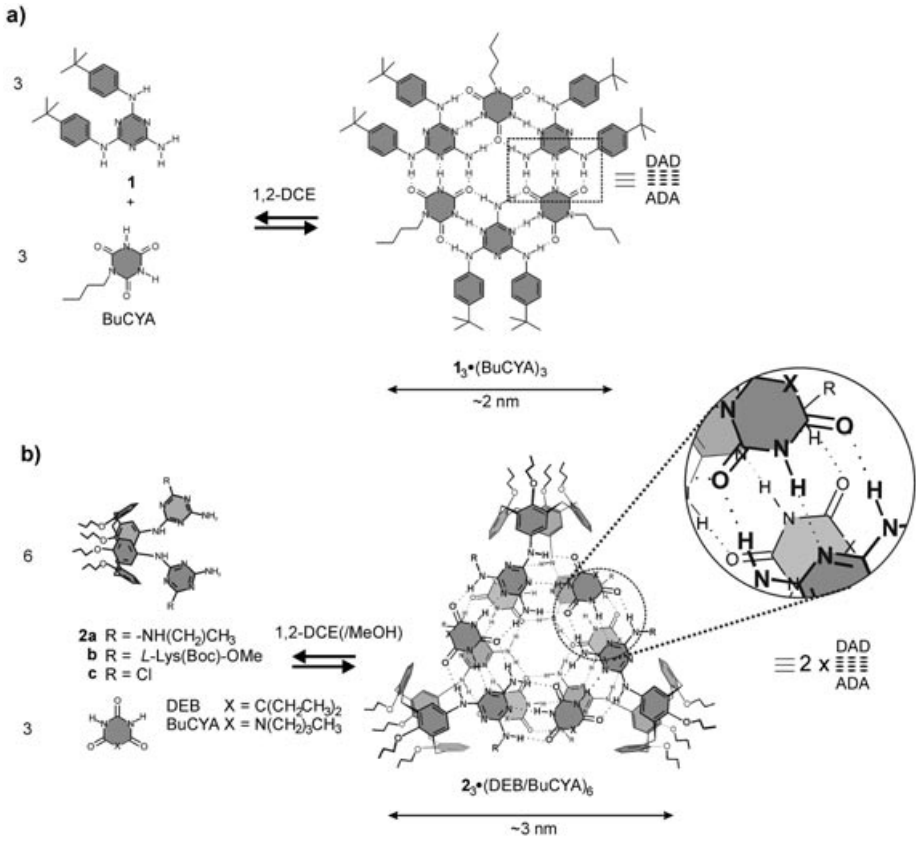

Scheme 1. Structures of melamine **1**, **2a–c**, DEB, and BuCYA and self-assembly of a) single rosette $\mathbf{1}_3\cdot(BuCYA)_3$; b) double rosettes $\mathbf{2a},\mathbf{b}_3\cdot(DEB/BuCYA)_6$. The magnification shows the DAD–ADA bonding motif present in the assemblies.

melamine units. Here, the calix[4]arene–dimelamines bear butyl or Boc-L-lysine methyl ester moieties, which form well-defined assemblies $\mathbf{2}_3\cdot(DEB/BuCYA)_6$ with two equivalents of 5,5′-diethylbarbituric acid (DEB) or *n*-butylcyanuric acid (BuCYA). Thus, the double rosette assemblies consist of three calix[4]arene–dimelamines and six DEBs (or BuCYAs) with 12 DAD–ADA interactions. Each dimelamine forms 12 hydrogen bonds (4×DAD) and each DEB (or BuCYA) six hydrogen bonds (2×ADA), giving a total of 36 hydrogen bonds within the assembly.[27–29] Double rosettes, as studied by ^{1}H NMR spectroscopy and MALDI-TOF-MS,[30–32] are stable in aprotic organic solvents such as dichloromethane, chloroform, benzene, and toluene even at 10^{-4} M. The high stability of this strong multiple DAD–ADA system makes it very useful for studying the influence of more polar solvents on hydrogen bonding. Previously our group reported association constants of 10^2 and 10^4 M^{-1} for melamine–barbiturate and melamine–cyanurate, respectively.[33] In addition, experiments in which chiral barbiturates in double rosettes were exchanged with achiral cyanurates[30] demonstrated that double rosettes with cyanurates are more stable than those with barbiturates. Quantification of the thermodynamics for self-assembly of double rosettes is therefore expected to reveal a higher stability for $\mathbf{2}_3\cdot(BuCYA)_6$ than for $\mathbf{2}_3\cdot(DEB)_6$.

Isothermal titration microcalorimetry (ITC) was used to determine thermodynamic parameters of these self-assembly processes. ITC is the only technique able to measure directly the change in bonding enthalpy ($\Delta H°$) for reversible interactions (very high or very low bonding constants are not directly accessible by ITC because of the steepness of the ITC titration curve or the requirement for high concentrations of the components, respectively). A more indirect method to determine thermodynamic parameters is van't Hoff analysis.[34] This method requires variable-temperature UV or NMR spectroscopy, with the approximation of assuming a zero heat capacity for the reaction. Besides measurement of $\Delta H°$, well-designed ITC experiments allow the calculation of formation constants K_f; therefore, appropriate treatment of ITC data can give a very detailed thermodynamic analysis. ITC has found widespread applicability within supramolecular chemistry, especially in host–guest recognition,[35–38] but to the best of our knowledge there have been no ITC studies of the assembly of multiple molecules into complex noncovalent systems.

Results and Discussion

Synthesis: Melamines **1** and **2a** were synthesized following literature procedures.[28,33] Compound **2b** was synthesized starting from calix[4]arenebis(chlorotriazine) **2c** (Scheme 1b).[28] Reaction of **2c** with an excess of *N*ε-Boc-L-lysine methyl ester hydrochloride and *N*,*N*-diisopropylethylamine (DIPEA) in THF at 90 °C for five days gave **2b** in 85 % yield.

Characterization of the corresponding double rosette by ^{1}H NMR spectroscopy,[30,31] confirmed the formation of the hydrogen-bonded assemblies $\mathbf{1}_3\cdot(DEB)_3$ and $\mathbf{2}_3\cdot(BuCYA/DEB)_6$.

Isothermal titration microcalorimetry: As a typical example, Figure 1 shows the results of an ITC measurement (298 K) of the formation of $\mathbf{2a}_3\cdot(BuCYA)_6$ by using 0.050, 0.075, and 0.10 mM solutions of BuCYA in 1,2-dichloroethane (1,2-DCE) in the ITC cell and with 0.25, 0.375, and 0.50 mM **2a** in 1,2-DCE as titrant, respectively.[39]

The strong heat effects measured when dimelamine **2a** was added to BuCYA clearly indicate that the self-assembly process is strongly enthalpy-driven. At all concentrations

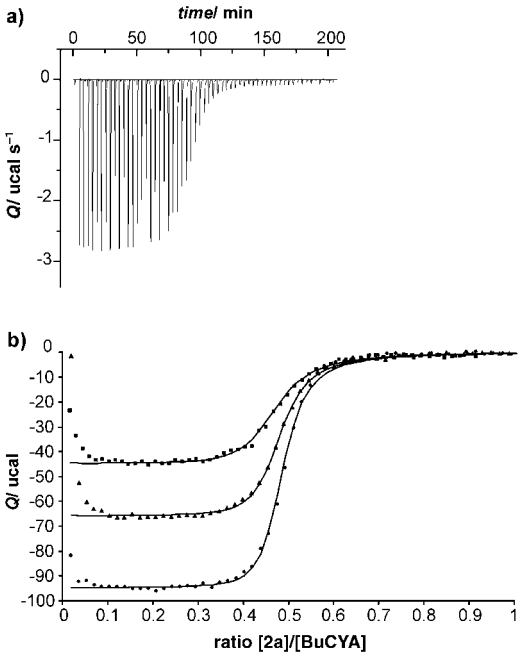

Figure 1. a) ITC measurement of the formation of $\mathbf{2a}_3$·$(BuCYA)_6$; cell: 0.075 mM BuCYA, burette: 0.375 mM **2a**. b) ITC titration curves obtained for formation of $\mathbf{2a}_3$·$(BuCYA)_6$: (■, cell: 0.050 mM BuCYA, burette: 0.250 mM **2a**; ▲, cell: 0.075 mM BuCYA, burette: 0.375 mM **2a**; ●, cell: 0.010 mM BuCYA, burette: 0.500 mM **2a**.

the ITC measurements indicate a 1:2 ratio for **2a**–BuCYA complex formation. This is consistent with the formation of a double rosette, in which three molecules of **2** and six molecules of BuCYA self-assemble. Furthermore, the concentration dependence of the ITC titration curves in these experiments is typical for high-order self-assembly processes.

To determine values of $\Delta G°$, $\Delta H°$, and $T\Delta S°$ from the observed heat effects, the ITC data have to be fitted to an appropriate bonding model. The process of rosette formation can be divided into two parts: first, the formation of linear aggregates between melamines and barbiturates (or cyanurates), and secondly the cyclization to rosette assemblies. In general, cyclization of linear aggregates is concentration-dependent and driven by entropy. For self-assembly processes the complex or aggregate with the lowest stoichiometry, in which the hydrogen bonds are used the most efficiently, is preferred. Furthermore, preorganization of the building blocks can stimulate the rosette assemblies to cyclize, because during the formation of the linear aggregates only minor conformational changes have to be made for cyclization to rosette assemblies and therefore the entropy change within the cyclization step is usually minimal. However, as favorable enthalpy changes due to hydrogen bonding will occur, cyclization is strongly induced. For the self-assembly of single and double rosettes, we have observed (with ^{1}H NMR spectroscopy and MALDI-TOF mass spectrometry) no species other than free melamine, free barbiturate (or cyanurate), and rosette assemblies in solution.[30,31]

For the equilibrium shown in Scheme 1a, this means that single rosette assemblies are formed directly from three melamines and three barbiturates, and that the formation constant K_f [M^{-5}] can be written as in Equation (1).

$$K_f = \frac{[\mathbf{1}_3 \cdot \mathrm{BuCYA}_3]}{[\mathbf{1}]^3[\mathrm{BuCYA}]^3} \quad (1)$$

Analogously, double rosette assemblies are directly formed from three calix[4]arene dimelamines and six barbiturates (or cyanurates), and the formation constant K_f [M^{-8}] can be written as in Equation (2).

$$K_f = \frac{[\mathbf{2}_3 \cdot \mathrm{BuCYA}_6]}{[\mathbf{2}]^3[\mathrm{BuCYA}]^6} \quad (2)$$

To analyze the ITC data obtained, a nonlinear least-squares minimization protocol was used in a 3:3 and 3:6 complexation model for single and double rosette assemblies, respectively. The heat effects, measured at all three concentrations, observed in the example shown in Figure 1 could be fitted to a 3:6 complexation model using $K_f = 2.7 \times 10^{43}$ and $\Delta H° = -123$ kcal mol^{-1} ($\Delta G° = -59$ kcal mol^{-1} and $T\Delta S° = -64$ kcal mol^{-1}). Consistency in the results of these calorimetric titrations at all three concentrations clearly indicates that the applied model is valid.

Self-assembly in apolar solvents

Single versus double rosettes: The results obtained after fitting the ITC data to the models described earlier are shown in Table 1. Because it is not possible to compare the K_f [M^{-5}] of single rosettes directly with the K_f [M^{-8}] of double rosettes,[40] we calculated the concentration (C_{50}) of assembly present when 50% of the components are incorporated in the complex (see Table 1).[41] Single rosette $\mathbf{1}_3$·$(BuCYA)_3$ with $C_{50} = 25$ μM is less stable than double rosette $\mathbf{2b}_3$·$(BuCYA)_6$ ($C_{50} = 7.1$ μM), indicating that double rosette assemblies are stable at lower concentrations. Furthermore, $\Delta H°$ for $\mathbf{2b}_3$·$(BuCYA)_6$ (−96 kcal mol^{-1}) is about twice that for $\mathbf{1}_3$·$(BuCYA)_3$ ($\Delta H° = -50$ kcal mol^{-1}). This implies that, in this case, the enthalpy change of double rosette assemblies is the sum of the enthalpy change of two single rosettes (formation of 36 (2×18) hydrogen bonds). In addition, for the double rosette $\mathbf{2a}_3$·$(BuCYA)_6$ the enthalpy change ($\Delta H° = -123$ kcal mol^{-1}) is about 2.5 times higher than for

Table 1. Thermodynamic parameters determined by ITC (298 K) for the self-assembly of single and double rosette assemblies in 1,2-DCE.

	K_f	$\Delta H°$ [kcal^{-1} mol^{-1}]	C_{50} [μM][a]	$\Delta G°$ [kcal^{-1} mol^{-1}]	$T\Delta S°$ [kcal^{-1} mol^{-1}]
$\mathbf{1}_3$·$(BuCYA)_3$	$(1.4 \pm 0.3) \times 10^{20}$ M^{-5}	−50 ± 5	25 ± 1	−27.5 ± 0.2	−23 ± 5
$\mathbf{2a}_3$·$(DEB)_6$	$(1.5 \pm 0.6) \times 10^{31}$ M^{-8}	−110 ± 2	23 ± 4	−42.3 ± 0.8	−68 ± 3
$\mathbf{2a}_3$·$(BuCYA)_6$	$(2.7 \pm 2.0) \times 10^{43}$ M^{-8}	−123 ± 11	0.7 ± 0.1	−59.1 ± 0.5	−64 ± 11
$\mathbf{2b}_3$·$(DEB)_6$	$(3.8 \pm 1.0) \times 10^{29}$ M^{-8}	−68 ± 5	35 ± 1	−40.3 ± 0.2	−28 ± 6
$\mathbf{2b}_3$·$(BuCYA)_6$	$(1.4 \pm 0.8) \times 10^{34}$ M^{-8}	−96 ± 1	7.1 ± 0.6	−47.9 ± 0.4	−49 ± 1

[a] See references [40,41].

the single rosette $\mathbf{1}_3$·(BuCYA)$_3$. In this case, the enthalpy change for the double rosette assembly is greater than the sum of those for two single rosettes, which may indicate additional complex stabilizing interactions.

For assembly $\mathbf{1}_3$·(BuCYA)$_3$ a $T\Delta S°$ of -22.5 kcal mol^{-1} was obtained, whereas for $\mathbf{2a}_3$·(BuCYA)$_6$ and $\mathbf{2b}_3$·(BuCYA)$_6$ $T\Delta S°$ values of -64.0 and -48.5 kcal mol^{-1}, respectively, were calculated. Single and double rosettes are built by assembling six and nine building blocks, respectively, leading to six and twelve enthalpic contributions for the six and twelve hydrogen-bonding arrays (DAD–ADA) being formed, whereas entropically the translational and rotational energies of only five or eight building blocks are restricted relative to the starting building block. The lower number of entropic contributions is clearly a direct consequence of the cyclization occurring in the assembly formation. When it is assumed that $T\Delta S°$ is determined merely by gathering of building blocks, the entropy factor for the association of one particle with another has to be the same for single and double rosettes, because each association consists of the same hydrogen-bonding arrays. For assemblies $\mathbf{1}_3$·(BuCYA)$_3$, $\mathbf{2a}_3$·(BuCYA)$_6$, and $\mathbf{2b}_3$·(BuCYA)$_6$, values of $T\Delta S° = -4.6$, -8.0, and -6.1 kcal mol^{-1} per additional building block are calculated, respectively. These data reinforce the hypothesis that assembly $\mathbf{2b}_3$·(BuCYA)$_6$ is basically a summation of two single rosette assemblies, where the stability is merely determined by hydrogen-bond formation and the gathering of building blocks. The somewhat higher unfavorable entropic contribution for $\mathbf{2b}_3$·(BuCYA)$_6$ can most probably be attributed to greater restriction of rotational mobility of the calixarene building blocks linking the two rosette planes than for the single rosette. Different entropic contributions per building block are obtained for $\mathbf{1}_3$·(BuCYA)$_3$ and $\mathbf{2a}_3$·(BuCYA)$_6$, which have identical hydrogen-bonding arrays. The somewhat higher enthalpy observed for $\mathbf{2a}_3$·(BuCYA)$_6$ (as mentioned above) is partially counterbalanced by higher unfavorable entropic contributions; this is a commonly observed enthalpy–entropy compensation effect (see below).

A possible explanation of the greater stability of assembly $\mathbf{2a}_3$·(BuCYA)$_6$ than $\mathbf{2b}_3$·(BuCYA)$_6$ ($C_{50} = 0.7\,\mu$M and 7.1 μM, respectively), and of its higher enthalpy change (Table 1), was illustrated by molecular modeling. Gas-phase molecular modeling (Quanta 97, CHARMm 24.0) shows that the two rosette motifs in $\mathbf{2a}_3$·(BuCYA)$_6$ are stacked on top of each other with an interatomic separation of 3.2 Å at the edges and 2.8 Å in the center of the rosette, whereas for $\mathbf{2b}_3$·(BuCYA)$_6$ the interatomic separation is 3.4 Å at the edges and 3.2 Å in the center (Figure 2). Consequently, the surface arrangement in $\mathbf{2a}_3$·(BuCYA)$_6$ can lead to better stacking and/or to hydrogen-bonding interactions between the two rosette layers. In addition, $T\Delta S°$ will be larger for $\mathbf{2a}_3$·(BuCYA)$_6$ than for $\mathbf{2b}_3$·(BuCYA)$_6$, because of restrictions in mobility due to formation of the additional interactions. The exact role of the different functionalities remains unclear, although steric or electronic influences from the bulkier lysine functionality are conceivable.

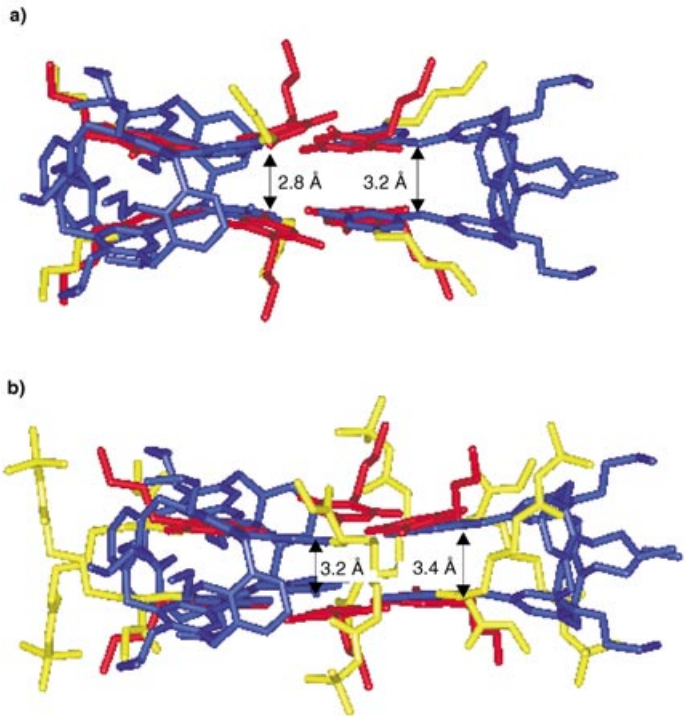

Figure 2. Gas-phase minimized structures: a) $\mathbf{2a}_3$·(BuCYA)$_6$; b) $\mathbf{2b}_3$·(BuCYA)$_6$.

Barbiturates versus cyanurates: Our group[33] has previously reported that the self-assembly of a melamine with a cyanurate (CYA) gives stronger complexes than between melamine and barbiturate (BAR), because of the higher acidity of the CYA. Association constants of 10^2 and $10^4\,$M^{-1} were reported for melamine–BAR and melamine–CYA, respectively. Double rosette assemblies contain 12 of these bonding motifs. Therefore, assemblies of $\mathbf{2}_3$·(BuCYA)$_6$ are expected to be more stable than the corresponding assemblies of $\mathbf{2}_3$·(DEB)$_6$.

Effectively, assemblies $\mathbf{2a}_3$·(DEB)$_6$ and $\mathbf{2b}_3$·(DEB)$_6$ exhibit lower K_f values than their BuCYA analogues (Table 1). The difference in $\Delta H°$ between $\mathbf{2b}_3$·(DEB)$_6$ and $\mathbf{2b}_3$·(BuCYA)$_6$ ($\Delta H° = -68.2$ and -96.4 kcal mol^{-1}, respectively) is mainly due to stronger hydrogen bonding provided by BuCYA. Differences between enthalpy as well as entropy changes are less pronounced between assemblies $\mathbf{2a}_3$·(DEB)$_6$ and $\mathbf{2a}_3$·(BuCYA)$_6$ ($\Delta H° = -110.2$ and -123.1 kcal mol^{-1}; $T\Delta S° = -67.9$ and -64.0 kcal mol^{-1}, respectively), supporting the hypothesis that the stability of double rosettes with **2a** are not determined only by the formation of 12 DAD–ADA bonding motifs but that additional stabilizing interactions may contribute.

Effect of solvent polarity on double rosette formation: ITC measurements with single rosette $\mathbf{1}_3$·(BuCYA)$_3$ and double rosettes $\mathbf{2a}_3$·(DEB)$_6$ and $\mathbf{2b}_3$·(DEB)$_6$ in MeOH/1,2-DCE mixtures were not possible. The low stability of these noncovalent complexes requires concentrations exceeding the solubility of the components. However, the high stability of double rosette assemblies $\mathbf{2a}_3$·(BuCYA)$_6$ and $\mathbf{2b}_3$·(BuCYA)$_6$, containing the cyanurate derivative, make them perfect can-

didates for stability studies by ITC. The thermodynamic parameters associated with formation of double rosette assemblies $\mathbf{2a}_3$·(BuCYA)$_6$ and $\mathbf{2b}_3$·(BuCYA)$_6$ in different MeOH/1,2-DCE solvent mixtures are shown in Table 2.

Table 2. Thermodynamic parameters determined by ITC (298 K) for the self-assembly of double rosette assemblies in different mixtures of 1,2-DCE and MeOH.

Assembly	MeOH in 1,2-DCE [%]	K_f [M^{-8}]	$\Delta H°$ [kcal^{-1}mol^{-1}]	C_{50} [μM][a]	$\Delta G°$ [kcal^{-1}mol^{-1}]	$T\Delta S°$ [kcal^{-1}mol^{-1}]
$\mathbf{2a}_3$·(BuCYA)$_6$	0	$(2.7\pm2.1)\times10^{43}$	-123 ± 11	0.7 ± 0.1	-59.1 ± 0.5	-64 ± 11
	10	$(9.7\pm1.1)\times10^{29}$	-71 ± 2	31 ± 0	-40.9 ± 0.1	-30 ± 2
	20	$(3.4\pm2.1)\times10^{26}$	-50 ± 1	84 ± 1	-36.2 ± 0.1	-14 ± 1
	50	$(5.6\pm5.0)\times10^{23}$	-38 ± 1	186 ± 2	-32.4 ± 0.1	-6 ± 1
$\mathbf{2b}_3$·(BuCYA)$_6$	0	$(1.4\pm0.8)\times10^{34}$	-96 ± 1	7.1 ± 0.6	-47.9 ± 0.4	-49 ± 1
	10	$(1.4\pm1.0)\times10^{27}$	-60 ± 5	71 ± 6	-36.9 ± 0.4	-23 ± 5
	20	$(4.2\pm3.0)\times10^{24}$	-46 ± 2	150 ± 20	-33.4 ± 0.6	-12 ± 1
	50	$(7.3\pm0.6)\times10^{21}$	-39 ± 2	320 ± 3	-29.8 ± 0.1	-9 ± 2

[a] See references [40, 41].

Compared with neat 1,2-DCE, the C_{50} values in a 1:9 mixture of MeOH/1,2-DCE increased from 0.7 and 7.1 μM to 31 and 71 μM for $\mathbf{2a}_3$·(BuCYA)$_6$ and $\mathbf{2b}_3$·(BuCYA)$_6$, respectively (Table 2). A further increase in the percentage of MeOH in 1,2-DCE led to a less dramatic increase in C_{50}. From the ITC measurements for both assemblies, when the percentage of MeOH is increased, a decrease in both enthalpy and entropy is observed. For the formation of $\mathbf{2a}_3$·(BuCYA)$_6$ and $\mathbf{2b}_3$·(BuCYA)$_6$ in neat 1,2-DCE, $\Delta H°$ values of -123 and -96.4 kcal mol^{-1}, respectively, were obtained. When 10% of MeOH was present these values were -70.5 and -59.8 kcal mol^{-1}, respectively. This loss in enthalpy was partly compensated by a less negative value for $T\Delta S°$ (from -64.0 to -29.6 kcal mol^{-1} and from -48.6 to -22.9 kcal mol^{-1}).

An enthalpy–entropy compensation (EEC) plot reflects how increasing favourable enthalpy is offset by a change in entropy or vice versa. When the entropy and enthalpy of formation for assemblies $\mathbf{2a}_3$·(BuCYA)$_6$ and $\mathbf{2b}_3$·(BuCYA)$_6$ at different ratios of MeOH in 1,2-DCE are plotted together, a straight line is obtained (Figure 3, solid line). Consequently the slope of the EEC plot coincides for both assemblies, meaning that the extent of compensation for the decrease in enthalpy of formation by lower entropy is identical for both assemblies. The slope of the EEC plot is 1.46; this means that the free energy of formation is more sensitive to changes in enthalpy.[42] A slope greater than unity suggests that when the percentage of MeOH in the solvent mixture is increased, eventually the decrease in enthalpy change cannot be compensated by entropy changes.[43] Nevertheless, for assemblies $\mathbf{2a}_3$·(BuCYA)$_6$ and $\mathbf{2b}_3$·(BuCYA)$_6$ this will only happen for strongly endothermic $\Delta H°$ values.

Correlation between solvent polarity and $\Delta G°$: With methanol as solvent, it was not possible to measure any appreciable heat effect for the formation of double rosettes $\mathbf{2a}_3$·(BuCYA)$_6$ and $\mathbf{2b}_3$·(BuCYA)$_6$ by ITC, because of the solubility limitations of dimelamines **2a** and **2b** and of BuCYA in this solvent. Therefore, to estimate the thermodynamic data for the formation of double rosettes in pure methanol (and other polar solvents), we used a theoretical model in which the solvent polarity is correlated with $\Delta G°$. For this purpose we determined the solvent polarity parameter E_T^N for solvent mixtures ranging from 0 to 100% MeOH in 1,2-DCE using UV/Vis measurements.[44,45]

A plot of $\Delta G°$ values from Table 2 for assemblies $\mathbf{2a}_3$·(BuCYA)$_6$ and $\mathbf{2b}_3$·(BuCYA)$_6$ against these E_t^N values resulted in a straight line for both assemblies (Figure 4), indicating a linear correlation between $\Delta G°$ and the polarity of the solvent (mixture). A steeper curve suggests a more pronounced (negative) effect on assembly stability

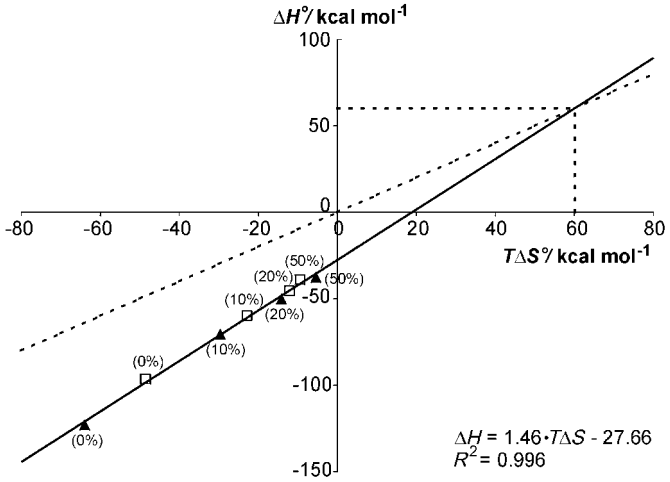

Figure 3. Solid line: enthalpy–entropy compensation (EEC) plot reflecting how increasing favorable enthalpy is offset by a change in entropy and vice versa. ▲: $\mathbf{2a}_3$·(BuCYA)$_6$; □: $\mathbf{2b}_3$·(BuCYA)$_6$. The percentages of MeOH in 1,2-DCE are indicated in parentheses. Broken line: behavior when the enthalpy changes are completely compensated by entropy changes.

upon an increase of solvent polarity. At $E_T^N = 0.76$ both assemblies exhibit the same change in free energy ($\Delta G° = -26.8$ kcal mol^{-1}). Coincidentally, the E_T^N value of MeOH is also 0.76, implying that assemblies $\mathbf{2a}_3$·(BuCYA)$_6$ and $\mathbf{2b}_3$·(BuCYA)$_6$ exhibit equal stability in pure MeOH ($C_{50} = 0.6$ mM).

Correlation of the solvent polarity with $\Delta G°$ provides $\Delta G°$ values for assemblies $\mathbf{2a}_3$·(BuCYA)$_6$ and $\mathbf{2b}_3$·(BuCYA)$_6$ in various solvents. From these values together with the equation describing the EEC plot, $\Delta H°$ and $T\Delta S°$ can be calculated for the formation of both assemblies. For both double rosettes in MeOH, $\Delta H° = -24.8$ kcal mol^{-1} and $T\Delta S° = 2.0$ kcal mol^{-1}. These data suggest that, based on solvent polarity, the self-assembly of $\mathbf{2a}_3$·(BuCYA)$_6$ and $\mathbf{2b}_3$·(BuCYA)$_6$ in methanol is possible. Surprisingly, in methanol this process is still mainly enthalpy-driven, although reinforced by entropic effects. Thus in MeOH the positive en-

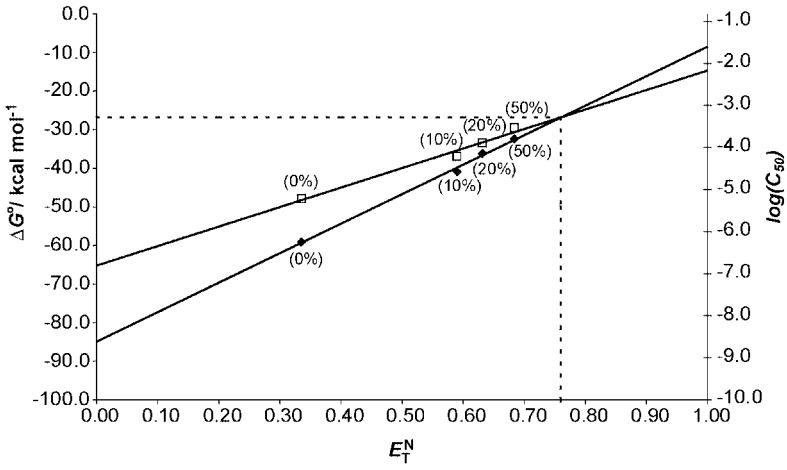

Figure 4. Effect of solvent polarity on $\Delta G°$ for assemblies $\mathbf{2a}_3$·BuCYA$_6$ (◆) and $\mathbf{2b}_3$·BuCYA$_6$ (□). ◆: $\Delta G° = 76.409\,E_T^N - 84.897$ ($R^2 = 0.996$), □: $\Delta G° = 50.503\,E_T^N - 65.86$ ($R^2 = 0.980$). The percentages of MeOH in 1,2-DCE are indicated in parentheses. The crossing point of the broken lines corresponds with formation of double rosettes in pure methanol.

thalpy of desolvation of solute molecules is not able to override the negative enthalpy for double rosette formation.

For double rosette formation in water ($E_T^N = 1.00$), $\Delta G°$ values of -8.5 and -14.7 kcal mol^{-1} for $\mathbf{2a}_3$·(BuCYA)$_6$ and $\mathbf{2b}_3$·(BuCYA)$_6$, respectively, were calculated, indicating that these two assemblies might also be formed in water. Calculated C_{50} values of 28.7 and 7.8 mM for $\mathbf{2a}_3$·(BuCYA)$_6$ and $\mathbf{2b}_3$·(BuCYA)$_6$ indicate that double rosette $\mathbf{2b}_3$·(BuCYA)$_6$, bearing the lysine moiety, exhibits greater stability in water.

Interestingly, calculated $\Delta H°$ and $T\Delta S°$ values for $\mathbf{2a}_3$·(BuCYA)$_6$ (33.2 and 41.7 kcal mol^{-1}, respectively) and for $\mathbf{2b}_3$·(BuCYA)$_6$ (13.5 and 28.2 kcal mol^{-1}, respectively), indicate that the formation of both double rosettes would be entropically driven in water, in which a positive enthalpy change is expected to arise from a positive enthalpy of desolvation, which overrides the expected negative enthalpy for double rosette formation. These results indicate that the solvation abilities of methanol and water are very different, but that assembly formation is possible, in principle, in both solvents.[46]

Double rosette formation in MeOH: As mentioned above, ITC measurements for the formation of double rosettes in MeOH are not possible. However, the theoretical thermodynamic profile obtained as described in the preceding section implies that double rosettes could be formed in this solvent.

To prove experimentally the formation of double rosette $\mathbf{2b}_3$·(BuCYA)$_6$ in MeOH we used ^{1}H NMR and CD spectroscopy. These techniques allow the use of more dilute solutions of the building blocks. Moreover, **2b** and BuCYA can be mixed directly in these techniques (ITC requires initially separate solutions of each component), leading to higher solubility of the double rosette than of the isolated components. Based on the $\Delta G°$ versus E_T^N plot, 97% formation of $\mathbf{2b}_3$·(BuCYA)$_6$ in [D$_4$]methanol was predicted from the free energy.

Mixing of dimelamine **2b** (3 μmol) and BuCYA (30 μmol) in [D$_4$]methanol (1 mL) resulted in clear solutions above 40 °C. Although precipitation occurred at lower temperatures, formation of double rosettes $\mathbf{2b}_3$·(BuCYA)$_6$ was observed by ^{1}H NMR spectroscopy (Figure 5). Because of rapid exchange, the ^{1}H NMR spectrum does not show the characteristic hydrogen-bonded protons[27] of the assembly in [D$_4$]methanol. However, the signal at $\delta = 5.9$ belongs to the aromatic proton (H$_d$) of the calix[4]arene moiety that is only present at this chemical shift when the assembly is formed. The percentage of assembly formed was determined by comparing the integrals of H$_d$ with the Ar–CH$_2$–Ar of the calix[4]arene moiety. This resulted in about 63% formation of $\mathbf{2b}_3$·(BuCYA)$_6$ in [D$_4$]methanol. The lower double rosette formation observed by ^{1}H NMR spectroscopy is probably due to some precipitation of the assembly (components) at 298 K.

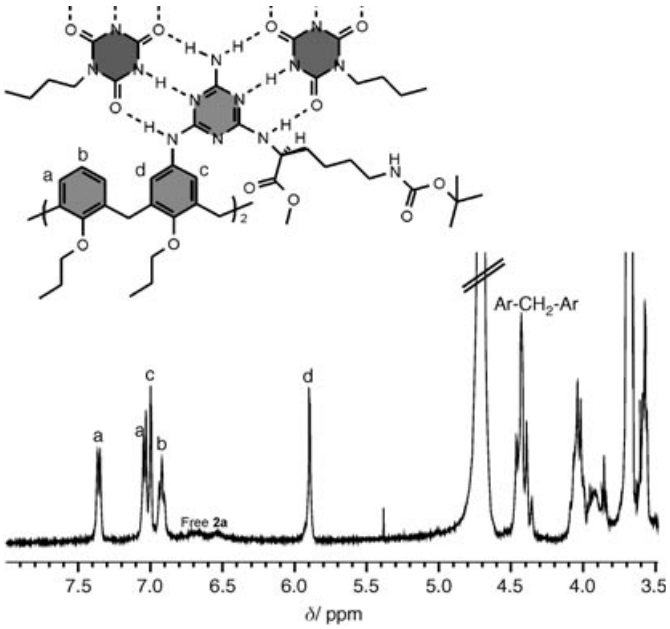

Figure 5. Part of the ^{1}H NMR spectrum of $\mathbf{2b}_3$·(BuCYA)$_6$ in [D$_4$]methanol at 300 MHz and 298 K.

Additionally, formation of double rosette $\mathbf{2b}_3$·(BuCYA)$_6$ in MeOH was demonstrated by circular dichroism (CD) spectroscopy. The dimelamine moieties in **2b** have chiral centers owing to the presence of the lysine residues. Subsequently, owing to complete induction of supramolecular chirality, the hydrogen-bonded assembly $\mathbf{2b}_3$·(BuCYA)$_6$ exists exclusively as a single diastereomer.[27–30] As a result, double rosette assemblies exhibit a very strong CD, while the individual components are hardly CD-active (Figure 6).

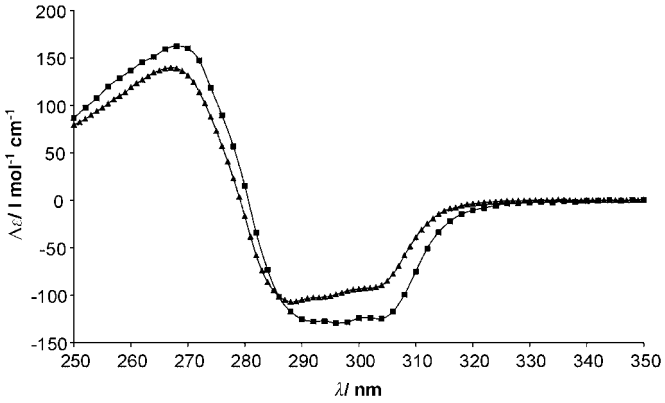

Figure 6. CD spectrum of $\mathbf{2b}_3$·(BuCYA)$_6$ in methanol (▲) and chloroform (■) at 298 K.

Both the ^{1}H NMR and CD spectra clearly prove that double rosette $\mathbf{2b}_3$·(BuCYA)$_6$ is formed in pure methanol.

Conclusion

The thermodynamic properties required for the formation of single and double rosettes were determined by ITC, which provides a facile and effective approach to measuring changes in bonding enthalpy and calculating other thermodynamic parameters for self-assembled systems. Depending on functionalities in the calix[4]arene–dimelamine moieties, it was found that the thermodynamics for the formation of double rosette assemblies can be either the sum for the self-assembly of two single rosette structures or the sum for two single rosettes reinforced by additional complex stabilizing interactions. As expected, double rosettes bearing cyanuric acid derivatives are more stable than the corresponding rosettes bearing barbiturate derivatives.

An increase in the solvent polarity decreases $\Delta G°$ and thereby results in less strong assembly formation. In all 1,2-DCE/MeOH solvent mixtures the negative effect of desolvation on $\Delta H°$ did not override the high favorable enthalpy of double rosette formation. Formation of double rosettes remained, therefore, enthalpy-driven.

Correlation of $\Delta G°$ energies with the solvent polarity indicated that it is possible to obtain double rosette assemblies in methanol and in water. As expected, the simulation shows that formation of double rosettes in water is entropy-driven rather then enthalpy-driven. However, to our surprise, double rosette formation in MeOH is still enthalpy-driven.

^{1}H NMR spectroscopy and CD spectroscopy proved that hydrogen-bonded double rosettes can be formed in neat methanol.

Experimental Section

General methods: THF was distilled from Na/benzophenone. All chemicals were reagent grade and used without further purification. NMR spectra were recorded on a Varian Unity 300 (^{1}H NMR 300 MHz) spectrometer in [D$_1$]chloroform or [D$_4$]methanol. Residual solvent protons were used as an internal standard, and chemical shifts are given relative to trimethylsilane (TMS).

FAB spectra were measured on a Finnigan MAT 90 spectrometer with *m*-nitrobenzyl alcohol (NBA) matrix. MALDI-TOF mass spectra were recorded on a PerSpective Biosystems Voyager-De-RP spectrometer. A 337 nm UV nitrogen laser producing 3 ns pulses was used in the linear and reflector modes. Elemental analyses were performed on a Carlo Erba EA1106 instrument. Calorimetric measurements were carried out in a Microcal VP-ITC microcalorimeter (cell volume 1.4115 mL). For each experiment the heat effect of 60 injections of 5 μL titrant was measured. Instrument settings were: injection duration 30 s, spacing 570 s, low feedback at 16.3 μcal s^{-1} reference power, temperature 25 °C. UV/Vis measurements were performed on a HP8452A diode array spectrophotometer using solvents of spectroscopic grade.

ITC measurements: Hydrogen bonds are less strong in 1,2-DCE than in $CHCl_3$,[47,48] because the dipole moment and dielectric constants of $CHCl_3$ ($\mu = 1.1$ D, $\varepsilon_r = 4.89$) are lower than those for 1,2-DCE ($\mu = 1.8$ D, $\varepsilon_r = 10.36$).[44] Nevertheless, to prevent errors incurred by evaporation, the ITC measurements were performed in 1,2-DCE at 298 K.

ITC measurements for the formation of $\mathbf{1}_3$·(BuCYA)$_3$ in 1,2-DCE were made in triplicate, with 1 mM solutions of melamine **1** in the cell and 10 mM BuCYA solutions in the burette. In this case, measurement at different concentrations was not possible, because of solubility problems at high concentrations of **1** and of BuCYA. Furthermore, at lower concentrations no assembly formation was observed. ITC measurements with $\mathbf{2}_3$·(DEB/BuCYA)$_6$ in 1,2-DCE were performed at three different concentrations with solutions of DEB or BuCYA in the cell and solutions of dimelamine **2a** or **2b** as titrants. The formation of $\mathbf{2a}_3$·(BuCYA)$_6$ and $\mathbf{2b}_3$·(BuCYA)$_6$ in solvent mixtures containing different percentages of MeOH in 1,2-DCE was also studied by ITC measurements in triplicate at MeOH/1,2-DCE ratios of 0, 0.1, 0.2 and 0.5. ITC curves were determined at two different concentrations depending on the amount of MeOH present.

UV/Vis measurements: E_T^N values were determined by measuring the absorbance changes of 2,6-diphenyl-4-(2,4,6-triphenyl-1-pyridino)phenolate (Reichardt's dye) upon increasing the percentage of MeOH in the MeOH/1,2-DCE mixture from 0% to 100%. Stock solutions of Reichardt's dye (0.12 mg mL^{-1}) in MeOH and 1,2-DCE were prepared and mixed to the desired MeOH/1,2-DCE ratios. For each solvent mixture three UV/Vis measurements were made and a blank was recorded.

Syntheses: The synthesis of **1**, **2a** and **2c** has been reported previously.[28,33]

*5,17-*N,N-*Bis[4-amino-6-[2-(6-*Nε*-Boc-aminohexanoic acid methyl ester)-amino]-1,3,5-triazin-2-yl]diamino-25,26,27,28-tetrapropoxycalix[4]arene (**2b**)*: *N*ε-Boc-L-lysine methyl ester hydrochloride (3.0 g, 10.2 mmol) and DIPEA (2.0 mL, 11.4 mmol) were added to a solution of bis(chlorotriazine) **2c** (1.0 g, 1.14 mmol) in freshly distilled THF (20 mL). This mixture was stirred at 90 °C for five days. The solution was cooled to room temperature. The product was precipitated in water (40 mL), and recrystallized from methanol. Pure dimelamine **2b** was obtained in 85% yield (1.28 g, 0.96 mmol). ^{1}H NMR ([D$_6$]DMSO): $\delta = 6.3$–6.05 (br m, 10H), 4.58–4.40 (br m, 2H), 4.3 and 3.1 (q, AB, $^2J_{HH} = 12.6$ Hz, 8H), 3.9 (t, $^3J_{HH} = 8.0$ Hz, 4H), 3.7–3.5 (br m, 10H), 2.96–2.78 (m, 4H), 2.0–1.8 (br m, 8H), 1.75–1.65 (m, 4H), 1.45–1.2 (br m, 26H), 1.07 and 0.87 ppm (t, $^3J_{HH} = 7.4$ Hz, 12H). MS (FAB): $m/z = 1327.9$ [M+H$^+$] (calcd 1327.7); elemental analysis calcd (%) for $C_{70}H_{98}N_{14}O_{12}$·0.65 MeOH: C 62.93, H 7.52, N 14.54; found: C 62.90, H 7.55, N 14.35.

Acknowledgements

This work has been partially financially supported by the Technology Foundation of the Netherlands (M.G.J.C.) and the Council for Chemical Sciences of the Netherlands Organization for Scientific Research (CW-STW). M.C.-C.s research has been made possible by a fellowship from the Royal Netherlands Academy of Arts and Sciences.

[1] The nature of the hydrogen bond depends on the distance between the donor (D) and acceptor (A) atoms, which in turn is dependent on their electronegativities.

[2] N. Takeda, K. Umemoto, K. Yamaguchi, M. Fujita, *Nature* **1999**, *398*, 794–799.

[3] Z. Zhong, H. Ikeda, M. Ayabe, S. Shinkai, S. Sakemoto, K. Yamaguchi, *J. Org. Chem.* **2001**, *66*, 1002–1008.

[4] D. K. Chand, K. Biradha, M. Fujita, *Chem. Commun.* **2001**, 1652–1653.

[5] K. Umemoto, K. T. H. Tsukui, K. Biradha, M. Fujita, *Angew. Chem.* **2001**, *113*, 2690–2692; *Angew. Chem. Int. Ed.* **2001**, *40*, 2620–2622.

[6] A. Ikeda, H. Udzu, Z. Zhong, S. Shinkai, S. Sakemoto, K. Yamaguchi, *J. Am. Chem. Soc.* **2001**, *123*, 3872–3877.

[7] E. Dalcanale, P. Jacopozzi, *Angew. Chem.* **1997**, *109*, 665–667; *Angew. Chem. Int. Ed. Engl.* **1997**, *36*, 613–615.

[8] F. Fochi, E. Wegelius, K. Rissanen, P. Cozzini, E. Marastoni, E. Fisicaro, P. Mannini, R. Fokkens, R. Dalcanale, *J. Am. Chem. Soc.* **2001**, *123*, 7539–7552.

[9] M. Fujita, S. Nagao, M. Iida, K. Ogata, K. Ogura, *J. Am. Chem. Soc.* **1993**, *115*, 1574–1576.

[10] M. Fujita, K. Umemoto, M. Yoshizawa, N. Fujita, T. Kusukawa, K. Biradha, *Chem. Commun.* **2001**, 509–518.

[11] O. Fox, N. K. Dalley, R. G. Harrison, *J. Am. Chem. Soc.* **1998**, *120*, 7111–7112.

[12] O. D. Fox, J. F. Y. Leung, J. M. Hunter, N. K. Dalley, R. G. Harrison, *Inorg. Chem.* **2000**, *39*, 783–790.

[13] L. S. Bok, J.-L. Hong, *Tetrahedron Lett.* **1998**, *39*, 4317–4320.

[14] M. Fujita, D. Oguro, M. Miyazawa, I. Oka, K. Yamagushi, K. Ogura, *Nature* **1995**, *378*, 469–471.

[15] J. L. Atwood, L. J. Barbour, A. Jerga, *Chem. Commun.* **2001**, 2376–2377.

[16] A. Shivanyuk, Jr. J. Rebek, *Chem. Commun.* **2001**, 2374–2375.

[17] M. O. Vysotsky, I. Thondorf, V. Böhmer, *Chem. Commun.* **2001**, 1890–1891.

[18] B. S. Lee, J.-I. Hong, *Tetrahedron Lett.* **1996**, *37*, 8501–8504.

[19] R. Fiammengo, P. Timmerman, F. De Jong, D. N. Reinhoudt, *Chem. Commun.* **2000**, 2312–2314.

[20] T. Grawe, T. Schrader, M. Gurrath, A. Kraft, F. Osterod, *Org. Lett.* **2000**, *2*, 29–32.

[21] B. Hamelin, L. Jullien, C. Derouet, C. H. de Penhoat, P. Berthault, *J. Am. Chem. Soc.* **1998**, *120*, 8438–8447.

[22] F. Corbellini, R. Fiammengo, P. Timmerman, M. Crego-Calama, K. Versluis, A. J. R. Heck, I. Luyten, D. N. Reinhoudt, *J. Am. Chem. Soc.* **2002**, *124*, 6569–6575.

[23] F. Corbellini, L. D. Costanzo, M. Crego-Calama, S. Geremia, D. N. Reinhoudt, *J. Am. Chem. Soc.* **2003**, *125*, 9946–9947.

[24] M. Mammen, E. E. Simanek, G. M. Whitesides, *J. Am. Chem. Soc.* **1996**, *118*, 12614–12623.

[25] In these studies the average value measured in chloroform for a hydrogen bond was used to estimate the free-energy index I_G.

[26] C. T. Seto, J. P. Mathias, G. M. Whitesides, *J. Am. Chem. Soc.* **1993**, *115*, 1321–1329.

[27] L. J. Prins , J. Huskens, F. De Jong, P. Timmerman, D. N. Reinhoudt, *Nature* **1999**, *398*, 498–502.

[28] P. Timmerman, R. H. Vreekamp, R. Hulst, W. Verboom, D. N. Reinhoudt, K. Risannen, K. A. Udachin, J. Ripmeester, *Chem. Eur. J.* **1997**, *3*, 1823–1832.

[29] R. H. Vreekamp, J. P. M. van Duynhoven, M. Hubert, W. Verboom, D. N. Reinhoudt, *Angew. Chem.* **1996**, *108*, 1306–1309; *Angew. Chem. Int. Ed. Engl.* **1996**, *35*, 1215–1218.

[30] L. J. Prins, F. De Jong, P. Timmerman, D. N. Reinhoudt, *Nature* **2000**, *408*, 181–184.

[31] K. A. Jolliffe, M. Crego-Calama, R. Fokkens, N. M. M. Nibbering, P. Timmerman, D. N. Reinhoudt, *Angew. Chem.* **1998**, *110*, 1294–1297; *Angew. Chem. Int. Ed.* **1998**, *37*, 1247–1251.

[32] L. J. Prins, K. A. Jolliffe, R. Hulst, P. Timmerman, D. N. Reinhoudt, *J. Am. Chem. Soc.* **2000**, *122*, 3617–3627.

[33] A. G. Bielejewska, C. E. Marjo, L. J. Prins, P. Timmerman, F. De Jong, D. N. Reinhoudt, *J. Am. Chem. Soc.* **2001**, *123*, 7518–7533.

[34] $\ln(K)$ is plotted against T^{-1}; $\ln(K_2/K_1) = -\Delta H/R(T_1^{-1} - T_2^{-1})$.

[35] S. L. Tobey, E. V. Anslyn, *J. Am. Chem. Soc.* **2003**, *125*, 10963–10970.

[36] S. L. Tobey , E. V. Anslyn, *J. Am. Chem. Soc.* **2003**, *125*, 14807–14815.

[37] B. R. Linton, M. S. Goodman, E. Fan, S. A. Van Arman, A. Hamilton, *J. Org. Chem.* **2001**, *66*, 7313–7319.

[38] M. V. Rekharsky, Y. Inoue, *Chem. Rev.* **1998**, *98*, 1875–1917.

[39] For a detailed description of the ITC experiments see the Experimental Section.

[40] Single rosettes are built up from six components, with the consequence that K_f values are expressed in M^{-5}, while double rosettes are built up from nine components and therefore K_f values are expressed in M^{-8}.

[41] Analogously to the dissociation constant K_d commonly employed for 1:1 complexes, C_{50} is defined as the concentration of assembly present when the components are mixed in the stoichiometry at which they are present in the complex and 50% of the components are incorporated in the complex. Therefore $K_f = C_{50}/((3\cdot C_{50})^3 \times (3\cdot C_{50})^3)$ for single rosette assemblies and $K_f = C_{50}/((3\cdot C_{50})^3 \times (6\cdot C_{50})^6)$ for double rosette assemblies.

[42] S. Sun, Md. A. Fazal, B. C. Roy, B. Chandra, S. Mallik, *Inorg. Chem.* **2002**, *41*, 1584–1590.

[43] The broken line in the EEC plot describes the behavior when the enthalpy changes are completely compensated by entropy changes. Beneath this line $\Delta G° < 0$, and above it $\Delta G° > 0$. At the point where the experimental line (solid) crosses the broken line $\Delta° = T\Delta S°$ and $\Delta G° = 0$.

[44] C. Reichardt, *Solvents and Solvent Effects in Organic Chemistry*, Wiley-VCH, Weinheim, **2003**.

[45] The term "solvachromism" is used to describe a pronounced change in position of a UV/Vis absorption band that accompanies a change in the polarity of the solvent. Large solvent-induced shifts of the visible $\pi \rightarrow \pi^*$ absorption band are observed for pyridinium *N*-phenolate betaine. This property has been used to introduce an empirical parameter of solvent polarity, $E_T(30)$, which is defined as the transition energy [kcal mol^{-1}] of the dissolved betaine dye: $E_T(30) = hc\nu N_A$, where h is Planck's constant, c the speed of light, ν the wavenumber, and N_A Avogadro's number. The number 30 is trivial and denotes the number of the dye when it was first reported. Hence, the normalized E_T^N value is dimensionless and defined as $E_T^N = [E_T(\text{solvent}) - E_T(\text{TMS})]/[E_T(\text{water}) - E_T(\text{TMS})]$, where water and TMS are used as extreme reference solvents. Hence, the E_T^N scale ranges from 0 for TMS, the least polar solvent, to 1 for water, the most polar solvent.

[46] Possibly the hydrophobic surface of the assembly is better solvated by the methyl groups of methanol and therefore results in less competition in hydrogen bonding.

[47] E. A. Archer, M. J. Krische, *J. Am. Chem. Soc.* **2002**, *124*, 5074–5083.

[48] J. N. Spencer, J. R. Sweigart, M. E. Brown, R. L. Bensing, T. L. Hassinger, W. Kelly, D. L. Housel, G. W. Reisinger, *J. Phys. Chem.* **1976**, *80*, 811–814.

Received: January 26, 2004
Published online: June 8, 2004

